Adv. Space Res. Vol. 10, No. 2, pp. (2)69–(2)79, 1990
Printed in Great Britain.

0273–1177/90 $0.00 +.50

HIGHLIGHTS FROM THE COS-B MISSION

W. Hermsen

Laboratory for Space Research Leiden, Niels Bohrweg 2, P.O. Box 9504, 2300 RA Leiden, The Netherlands

ABSTRACT

The European Space Agency's high-energy (E>50 MeV) gamma-ray observatory COS-B was operational from August 1975 to April 1982 and in that time made 65 observations of about 1 month duration and with a field-of-view of approximately 0.4 sr each. The high counting statistics achieved over the total mission allowed, for the first time, a detailed study of 1) the Galactic diffuse large-scale gamma-ray emissivity, 2) the small-scale gamma-ray structures caused by point-like sources and molecular clouds, and 3) the spectral and temperal behaviour of the Crab and the Vela pulsars. COS-B discovered the first high-energy extragalactic gamma-ray source (3C273) and resolved for the first time the emission from some local cloud complexes, notably the Orion-Monoceros and the Ophiuchus cloud complexes. For the latter case, in the Ophiuchus/Upper-Scorpius region there is circumstantial evidence for gamma-ray emission from molecular gas that was photodissociated after the passage of a SN shell.

INTRODUCTION

As early as May 1969 the experiment conceived for the COS-B satellite was proposed to the European Space Research Organisation (ESRO, predecessor of the European Space Agency, ESA). After the formal approval in July 1969 of a single spark-chamber experiment capable of detecting gamma rays of energies greater than about 50 MeV, six institutes forming the Caravane Collaboration together constructed and tested the instrument and were responsible for the selection of the observation program, the analysis of the data and the publication of the results. The members were:

* Max-Planck-Institut für Extraterrestrische Physik, Garching-bei-München, Federal Republic of Germany;
* Service d'Astrophysique, Centre d'Etude Nucleaires de Saclay, Gif-sur-Yvette, France;
* Laboratory for Space Research Leiden, Leiden, The Netherlands;
* Istituto di Fisica Cosmica del CNR, Milano, Italy;
* Space Science Department of the European Space Agency, ESTEC, Noordwijk, The Netherlands;
* Istituto di Fisica Cosmica e Informatica del CNR, Palermo, Italy.

This long-lasting collaboration was finished in 1985 when the final data base became publicly available /1/.

During the construction phase of COS-B the NASA satellite SAS-2 performed an almost complete survey of the Galactic plane and provided for the first time firm measurements of gamma-ray point sources such as the Crab /2/ and Vela /3/ pulsars and the strong gamma-ray source Geminga /4/ in the anti-centre direction. Unfortunately, this experiment failed after only seven months.

The COS-B telescope during its lifetime of about seven years could increase the counting statistics in gamma-ray astronomy by more than an order of magnitude. Furthermore, the inclusion of a spectrometer, providing energy measurement capability up to GeV energies, and the improvement in angular resolution selecting higher energy photons (average angular resolution for energies above 100 MeV about 2.5° FWHM), caused a quantum leap in the sensitivity-resolution plane.

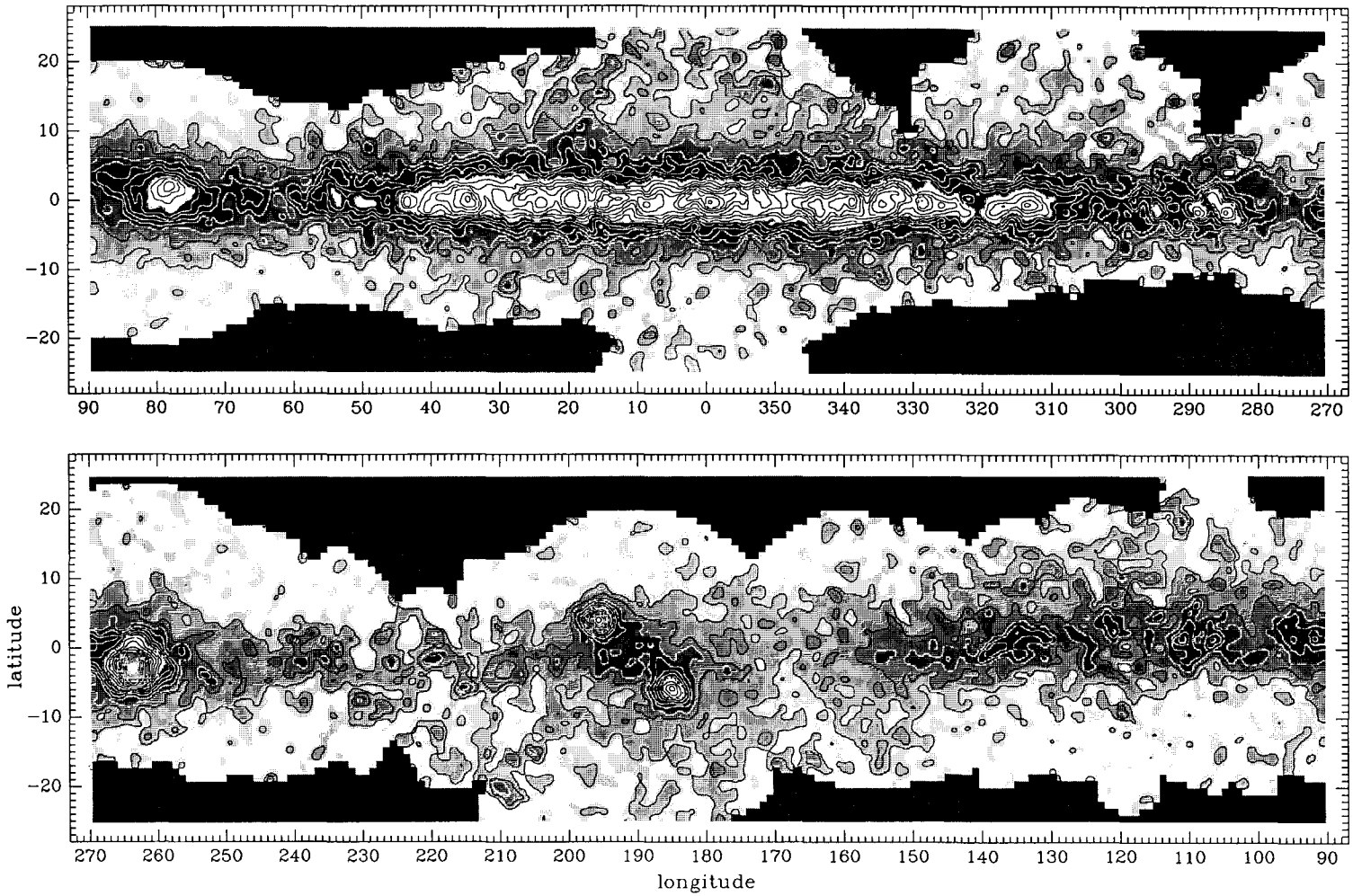

Fig.1. Gamma-ray intensity map of the Galactic disk derived from the final COS-B data base. The energy range is 100 MeV to 6 GeV. Contour lines are indicated at multiples of 5×10^{-5} photon cm^{-2} s^{-1} sr^{-1}. An isotropic background level of 8×10^{-5} ("on axis" /9/), largely of instrumental origin, has been subtracted. The dark areas at the edges of the map correspond to regions with an exposure $< 4 \times 10^{7}$ cm^{2} s (corresponding to roughly 15 days of observing time).

In this review a selection of key results will be presented. A pre-launch description of the satellite and telescope is given by Bignami et al. /5/ and Scarsi et al. /6/. The in-flight performance has been discussed by Hermsen /7/, Bloemen /8/ and Strong et al. /9/.

THE GAMMA-RAY SKY

An important achievement by the COS-B mission was the complete coverage of the Galactic plane region with a high exposure up to $|b| \leq 20°$. Figure 1 shows a Milky Way map for energies between 100 MeV and 6 GeV. This large-scale picture is dominated by the diffuse gamma-ray emission originating predominantly from the interaction of relativistic cosmic rays (CR) with the nuclei in the interstellar medium (ISM) (see e.g. Stecker /11/). Fine-scale structure down to 1°-2° has been proven to be real /7,12,13/ and mimics largely the clumpy molecular hydrogen distributon (/14/ and next section). Some strong gamma-ray sources are evident, such as the earlier discovered Vela ($l \approx 263°$), Crab ($l \approx 185°$) and Geminga ($l \approx 194°$) sources. The search for additional point-like sources is hampered by the structured background distribution and the success depends strongly on the accuracy of the model for the diffuse background radiation.

At intermediate latitudes ($10° < |b| < 20°$) the gamma-ray sky is dominated by the local ISM distribution /15,16,17/. However, the gamma-ray structures are only clearly resolved for the closest and most massive molecular cloud complexes, such as those in the Orion-Monoceros /18/ ($l \approx 200°$-$215°$, $b \approx -15°$) and the Ophiuchus regions /19/ ($l \approx 350°$-$360°$, $b \approx 15°$).

DIFFUSE GALACTIC GAMMA-RAY EMISSION

The study of the diffuse Galactic gamma-ray emission in the COS-B energy range is essentially a study of the Galactic distribution of the ISM, predominantly HI and H_2, and that of CR nuclei and electrons. The gamma-ray production in this energy range is, as stated above, dominated by CR-ISM interactions. Inverse Compton gamma rays resulting from the scattering of CR electrons on lower energy photons (optical, infrared, and 2.7 K relic) contribute a minor fraction /20/. Therefore, the Galactic diffuse gamma-ray distribution traces the product of the ISM density and CR density; π^0-decay gamma rays resulting from nucleus (GeV protons)-nucleus interactions dominating roughly at higher COS-B energies (E>150 MeV) and electron-Bremsstrahlung gamma rays from electron ($\leq$1 GeV)-ISM nucleus interactions dominating in the lower energy band (70-150 MeV).

When maps of independent tracers of the ISM are available, such as 21-cm radio data measuring accurately the HI distribution, and mm CO measurements tracing the H_2 distribution, a correlation study can be performed with the gamma-ray large scale distribution, rendering the Galactic gamma-ray emissivity (production rate per hydrogen atom) distribution. Such a distribution at higher energies is indicative for the Galactic distribution of the nucleonic (proton) component of the CR's and at lower energies of the electron component. Considering these Galactic CR distributions in relation to CR diffusion models, the remaining puzzle regarding the origin (sources) of the relativistic CR's can be addressed (see e.g. Bloemen, these proceedings; recent reviews on this topic can be found in /10,21,22/). Finally, such a correlation study quantifies the need for a point-source component to explain the total gamma-ray distribution.

The Caravane Collaboration addressed in a series of papers /14,23,24,25/ this topic, correlating the HI and CO distributions with the gamma-ray data, exploiting the distance information available in the radio - and mm data. The main goal of this work was to derive the Galactic gamma-ray distribution, assumed to be circularly symmetric, at different energy intervals and to calibrate the conversion factor between the velocity integrated CO line intensity, W(CO) and the H_2 column density, $N(H_2)$: $X = N(H_2)/W(CO)$. The latter calibration renders a 'gamma-ray' estimate of the total Galactic molecular hydrogen mass and its distribution.

Of particular interest in this work were tests for a possible energy dependence of the galactocentric radial gamma-ray emissivity (q) distribution and the factor $Y = [q(H_2)/q(HI)]X$. An energy dependence of the latter would signify a difference between the gamma-ray emissivity of HI and H_2, indicating an enhancement of CR's in, or exclusion from molecular clouds.

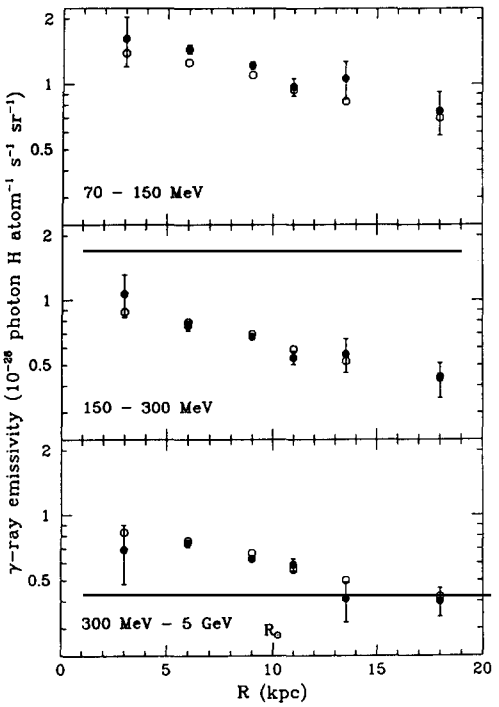

Fig.2.

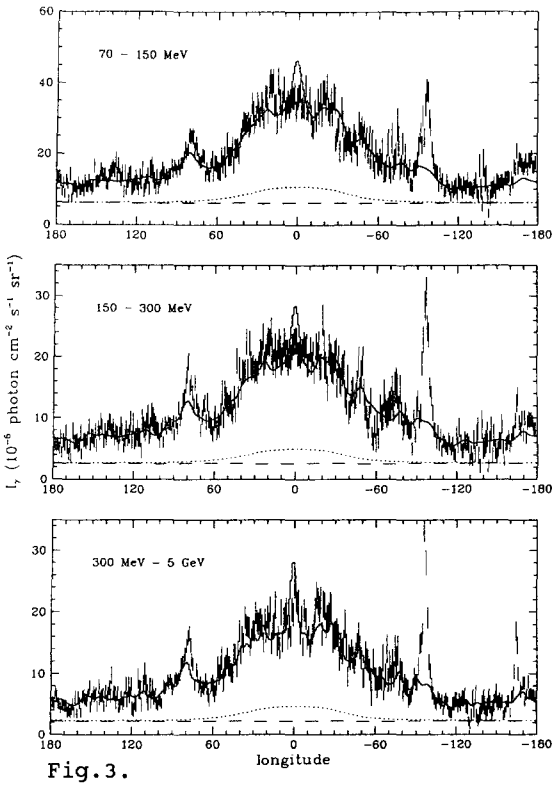

Fig.3.

Fig.2. Galacto-centric distribution of the gamma-ray emissivity obtained from a correlation analysis of HI, CO, and gamma-ray data /14/. *Circles:* Shape of the radial distribution is adopted to be independent of gamma-ray energy; the observed large-scale spectral variation along the Milky Way is attributed to an energy dependence of the parameter Y (see text). *Black dots:* Vice versa: Y adopted to be energy independent; spectral variation attributed to an energy dependence of the shape of the radial distribution.

Fig.3. Longitude distributions of the observed (±1 standard deviation error bars) and modelled (histogram) gamma-ray intensity, averaged over $|b|<5°$ /14/. The dotted line indicates the contribution from inverse-Compton emission to the model. The isotropic background is indicated by the dashed line. The specific model shown here has an energy-independent shape of the emissivity distributions (circles in Figure 2), but appears almost identical in this presentation for an energy-dependent shape (black dots in Figure 2).

Figure 2 shows the derived radial emissivity distributions /14/. The correlation studies indicated the need for an energy dependent model, but could hardly discriminate between an energy dependence of q or Y; both cases giving an equally good fit to the gamma-ray distribution. The latter model is slightly favoured (see discussion by Strong and colleagues /14/) and the agreement with the COS-B data is depicted by the longitude distributions in Figure 3. In conclusion: a good quantitative fit to the measured Galactic gamma-ray intensity distribution is obtained over the entire Galactic plane using the HI and CO distributions, and a small galactocentric gradient in the gamma-ray emissivity per hydrogen atom, and as such also in the CR density distribution (exponential scale length of approximately 10-15 kpc for electrons **and** nuclei (protons)). The average ratio of H_2 column density to integrated CO temperature is estimated to be $(2.3\pm0.3) \times 10^{20}$ molecules cm^{-2} (K km s^{-1})$^{-1}$ (This value is an upper limit if a population of unresolved gamma-ray sources exists with an angular distribution similar to that of the molecular gas, or if the cosmic-ray density is enhanced in molecular clouds). The corresponding mass of molecular hydrogen in the inner Galaxy, derived using both 1st and 4th quadrants, is 1.0×10^9 $M_\odot$.

The Durham group performed related studies on the SAS-2 and COS-B data /26,27,28/. Although some details of their works cannot be reconciled with the findings of Strong, Bloemen and colleagues, the main conclusions are in

agreement: large exponential scale lengths for electrons and nuclei, and a relatively low, compared to earlier estimates, amount of molecular hydrogen in the inner Galaxy (≤ total amount of HI). For a discussion of the differences see some recent reviews (/10,21,22/).

At intermediate latitudes ($5° \leq |b| \leq 20°$) in the inner Galaxy direction it appears that almost half of the observed gamma-ray intensities cannot be explained by CR-matter interactions. There is circumstantial evidence for an Inverse-Compton gamma-ray halo, presented by Bloemen in these proceedings. Alternative interpretations involve an enhancement due to the Loop I SNR /29/, and to the presence of the local spiral arm /30/.

THE LARGE COMPLEXES OF CLOUDS IN ORION/MONOCEROS AND OPHIUCHUS

The study of nearby cloud complexes gives contemporary gamma-ray astronomy with its modest angular resolution and counting statistics the unique opportunity to study dense active regions in which star formation is still going on, to verify the expectations from CR-matter interactions and to search for possible enhancements in CR density in these complexes.

From an analysis of SAS-2 data, Fichtel and colleagues /31/ had already suggested that a gamma-ray enhancement could be seen from the general direction of Gould's belt at distances varying up to 450 pc from the Sun. Early analysis of COS-B data /32/ established this finding, and, in addition, a significant excess was detected in the direction of the Ophiuchus dark cloud complex (distance about 130 pc) /13/. Morfill and colleagues /33/ compared the reported flux with mass estimates for the Rho Oph dark cloud and concluded that an enhancement in cosmic-ray density by a factor of about 3 was required, or that the mass and/or distance estimates were wrong. They suggested that the gamma-ray source may be the result of the acceleration of Galactic cosmic rays by an old supernova remnant (the North Polar Spur, Loop I, radius ±115 pc) and its interaction with the Rho Oph cloud. However, after more COS-B data on the region became available, Hermsen and Bloemen /19/ showed that the general structure of the Ophiuchus cloud complex, as delineated in extinction maps and OH data, was in fact resolved in gamma rays. A comparison between the total mass estimated from OH data /34/ and the gamma-ray flux from the total complex indicated that the measured gamma-ray flux is at most a factor 2 higher than expected, assuming cosmic rays of local density throughout the complex. Given the large experimental uncertainties, this was considered to be insufficient evidence for a local CR enhancement. Furthermore, the Orion cloud complex was also found to be resolved in the COS-B gamma-ray maps, clearly showing the northern and southern complexes L1630 and L1641 /35/.

After completion of the Columbia CO surveys of these cloud regions, it became feasible to perform detailed correlation studies between the gamma-ray data and CO and HI maps. CO data became first available for the Orion/Monoceros region /36/, and the correlation study /18/ showed a good two-dimensional correlation between the gamma-ray emission and the total gas distribution, explaining the former in terms of interactions of the gas with cosmic rays of local density, distributed uniformly in this region.

Recently, a complete CO survey of the Ophiuchus region also became available /37/. Figure 4 shows the measured gamma-ray distribution using all available COS-B data on this area for energies between 100 MeV and 6 GeV, as well as the integrated HI column density map and the velocity integrated CO antenna temperature ,W(CO), distribution. The gamma-ray 'beam' is significantly broader than those at radio - and mm wavelengths. Nevertheless, significant structure is visible in the gamma-ray data, showing particularly the molecular cloud complex. Using the $N(H_2)/W(CO)$ conversion factor and the gamma-ray emissivities determined for the solar neighbourhood in the large-scale correlation study, it can be shown that the gamma-ray intensities predicted for the molecular clouds as traced by CO data are fully consistent with the measurements: There is no indication for an enhancement of cosmic rays inside these clouds. However, the gamma-ray structure appears to be more extended towards somewhat lower longitudes and higher latitudes, already visible in the early map of Hermsen and Bloemen /19/. Therefore, a map of the differences between the predicted structure (using Figures 4b, 4c) and the measurements (Figure 4a) has been determined (Figure 4d). Care has been taken that no significant negative fluctuations are present with respect to the predictions, by adjusting the scaling parameters locally within their uncertainties. Figure 4d shows that at the positions of intense CO emissions the distribution is consistent with zero intensity, but that adjacent to the

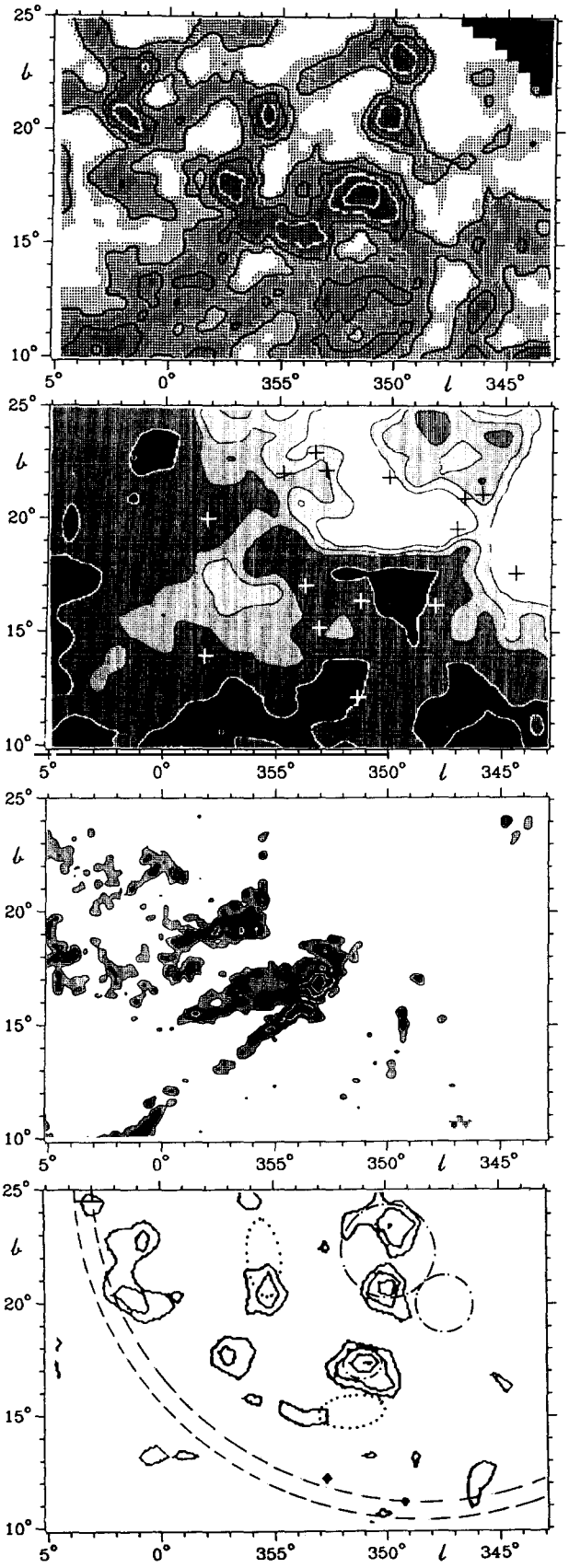

Fig.4. The Ophiuchus region:

a) Gamma-ray intensities for energies between 100 MeV and 6 GeV. Contour lines, background subtraction, dark area in corner: see Figure 1.

b) Integrated HI column density, contour values 12.5, 13.5, 14.5, 17.5, and 20 x 10^{20} cm^{-2}. Positions of the brightest stars (earlier than B2) are plotted as plusses (from /37/).

c) Velocity-integrated CO antenna temperature W(CO) for $-8<v<20$ km s^{-1}. Contour values: 5.0, 20.0, 55.0, and 112.5 K km s^{-1} /37/.

d) Differences between the observed (*a*) and the predicted diffuse emission based on the HI and CO surveys and the model parameters deduced by Strong et al. /14/. Energy range 100 MeV to 5 GeV. For the subtraction method see Bloemen /10/. Contour levels: 8.2, 13.1, 18.1 x 10^{-5} photon cm^{-2} s^{-1} sr^{-1}. The dash-dotted circles outline the HII regions in Sharpless's catalogue (1959); the dotted lines show some bright nebula from Lynds's catalogue (1965). The dashed circle segment sketches the position of an expanding shell of radius 40 pc /37/ which was interacting with the Ophiuchus complex, overtaking the clouds.

cloud structures, e.g. at about $(l,b)=(351°,18°)$ and at somewhat higher latitudes, excesses remain visible. The first excess coincides with a HII region and with a considerable amount of dust, visible in IR maps, /37/.Also the excesses at about $(l,b)=(350°,22°)$ are spatially consistent with HII regions and regions with a considerable amount of dust emission with practically no CO present. Again, the reflection nebula at about $(l,b)=(355°,22°)$ is spatially correlated with a dust cloud.

Evidently, there appear to be some features in the gamma-ray data which are not explained by CO and HI structures. From a detailed study of the stars and the interstellar medium of the Scorpio-Centaurus OB association, de Geus /37/ recently pointed out that a HI shell (radius about 40 pc) around the stars in Upper Scorpius appears to be created by stellar winds of the early type stars present in Upper Scorpius (indicated in Figure 4b) and by a supernova explosion of a massive star of about 40 $M_\odot$ and about 1 Myr ago. The detailed structure of the interstellar medium, including the elongated CO structures can be explained as being due to the passage of the SN shock (the approximate position has been sketched in Figures 4c,d, although in this region the spherical bubble representing the HI shell has been disturbed due to the interaction with the cloud complex).

Discussing the HII and IR structures at $(l,b)=(351°,18°)$ and taking into account the presence of a strong UV field, de Geus concluded that part of the Rho Oph molecular cloud that was originally located in this region has been photodissociated after the passage of the shock front. A similar conclusion can be drawn on the structures around $(l,b)=(350°,22°)$: a photodissociated remnant of a molecular cloud. Blandford and Cowie /38/ discussed the scenario of a dense cloud overtaken by a strong supernova blast wave, in which dissociated molecules behind the shock, in a medium of enhanced gas and magnetic field density, are predicted to show up in gamma rays. The important question arises: Do we need an enhancement in CR density inside this shell structure to explain the excess gamma-ray flux? Taking the preliminary mass estimates by de Geus, an enhancement in CR density of about an order of magnitude would be required. However, it is difficult to propose a CR enhancement in the dissociated molecular clouds due to this scenario, since, in the CO complex, which is also overtaken by the shock, no enhancement is found, but would then be expected.

Another possible explanation of the gamma-ray excesses is the production of Inverse Compton gamma rays due to electron photon interactions in the enhanced photon fields around the early type stars which ionized the ISM locally. The enhancements in photon density around the stars, together with some enhancement in electron density in the ionized medium around the stars, could be sufficient to explain the gamma-ray excesses. However, more accurate experimental data is required, such as more detailed mass estimates, and better spectral information in the gamma-ray domain. The Soviet-French Gamma-1 mission, and particularly the NASA GRO mission will provide such accurate estimates to discriminate between the different production mechanisms. It is noted that Pollock /39/ proposed the identification of two unresolved and so far unidentified gamma-ray sources, notably the strong source in the Cygnus region 2CG078+01, coinciding with the radio-bright SNR G78.2+2.1, in the framework of the scenario described by Blandford and Cowie.

COS-B GAMMA-RAY SOURCES

One of the highlights early in the mission was the discovery of significant small-scale structures in the gamma-ray maps. A 'CG' /12/ and a '2CG' gamma-ray source catalogue /7,13/ were established, applying a cross-correlation analysis /7/ to the data. Genuinely compact sources and sources of angular extent up to about 2° cannot be distinguished due to the modest COS-B angular resolution.

The 2CG catalogue contains 25 entries, including the well-known Vela and Crab radio pulsars, the Rho Oph cloud (later found to be resolved), and the only detected extra-galactic high-energy gamma-ray source 3C273 /40,41,42/. The remaining sources have not been unambiguously identified, including the enigmatic source Geminga (2CG195+04), and the strong source 2CG078+01 in the Cygnus region. In Figure 3 the strongest sources are clearly seen above the model prediction for the diffuse gamma-ray background. It is interesting to note that all gamma-ray sources,including the radio pulsars, the quasar and the unidentified sources such as Geminga, reach their maximum luminosity in the gamma-ray domain.

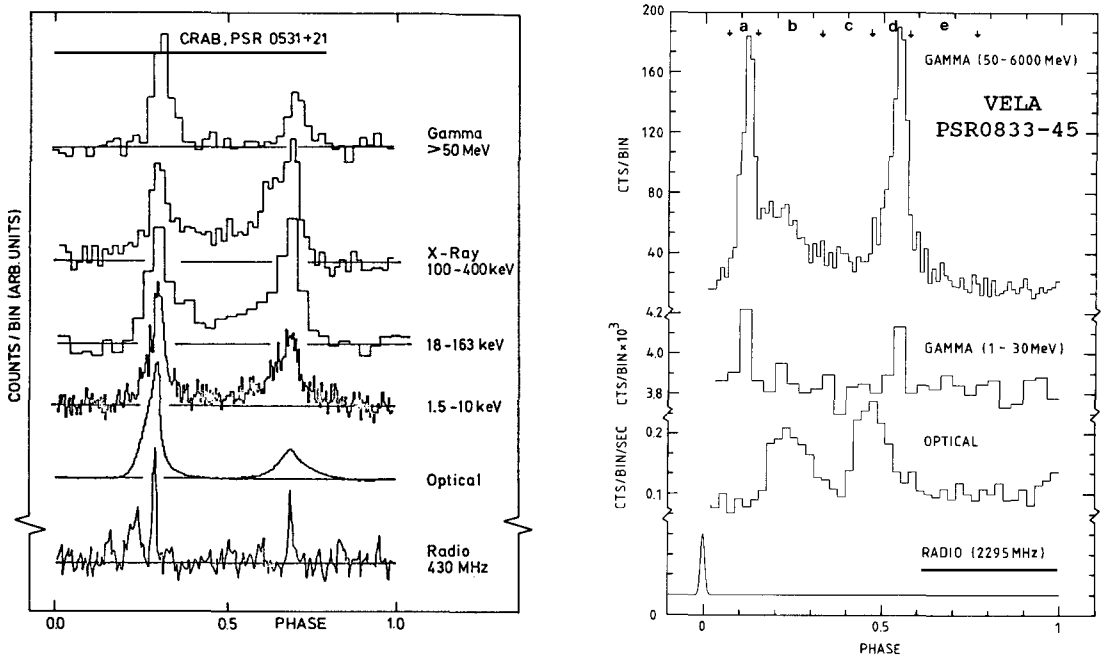

Fig.5. Lightcurves detected from Crab (PSR0531+21) and Vela (PSR0833-45) in different energy domains of the electro-magnetic spectrum (for references see /43/ and /47/, respectively). The Vela phase intervals selected for Figures 6 and 9 are indicated.

A significant problem in the search for counterparts at other wavelengths was the large positional uncertainty (0.4°-1.5° error radius). Furthermore, large-scale Galactic CO surveys were not yet available and it was impossible to discriminate either compact objects or local strong enhancements in cosmic-ray density from point-like sources which are due to the structured molecular gas distribution. Bignami and Hermsen /43/ reviewed many of the theoretically and experimentally proposed identifications.

The good fit of the model for the diffuse gamma-ray emission to the total intensity distribution shown in Figure 3, indicates that the component due to compact objects or to active regions in which the cosmic-ray density is locally enhanced, constitutes a minor fraction, probably less than 20%. The first attempt to search systematically for point-like features on top of the diffuse gamma-ray background was based on a maximum likelihood analysis /44,45/, so far applied to part of the Galactic plane region and for energies above 300 MeV only. The complete region has been analysed for energies above 70 MeV using again the cross-correlation analysis, subtracting in this case the model of Strong and colleagues /14/ for the diffuse emission (see Mayer-Hasselwander and Simpson, these proceedings). The two approaches have somewhat different sensitivities, but it appears that approximately 50% of the 2CG sources are due to compact objects or small-scale active regions, and that some new sources appear.

THE CRAB AND VELA GAMMA-RAY PULSARS

The only radio pulsars detected in high-energy gamma rays so far are the young pulsars Crab and Vela. The accumulation of the data by COS-B over a period of 6.7 years has allowed a study of the temporal behaviour of the pulsed gamma-ray flux from PSR0531+21 and PSR0833-45. The first was in the COS-B field-of view during six observation periods, each lasting for a duration of approximately 30-40 days, and the latter during ten periods. All data collected in the final COS-B data base on CRAB and Vela are used by Clear et al. /46/ and Grenier et al. /47/, respectively, to study the emission from these sources in great detail. Particularly the unprecedented high total exposure allowed an accurate determination of the time averaged phase histograms and of the time averaged spectra. Figure 5 shows the gamma-ray phase histograms of the two pulsars in comparison with the measured distributions at other wavelengths. The similarity of the Crab phase histogram over practically the entire electromagnetic spectrum is in strong contrast to the changing signature of Vela, which, remarkably, has only been

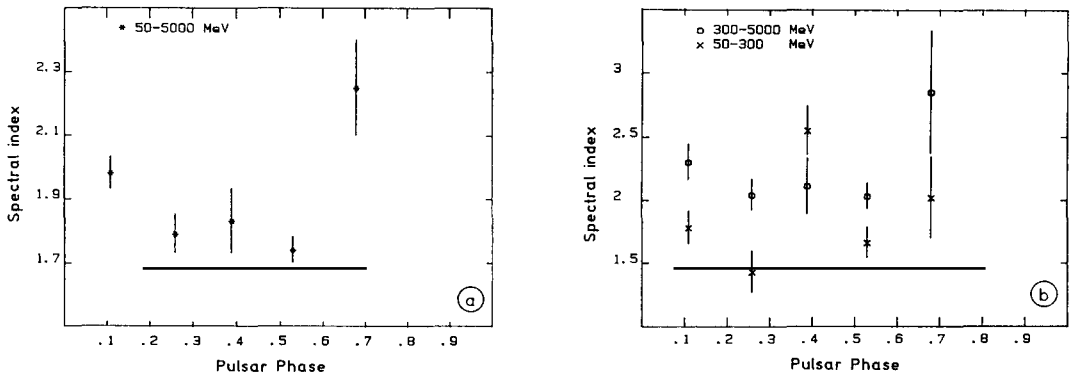

Fig.6. Time-averaged pulsed spectral index as a function of phase for the Vela pulsar; (a) one-power-law fit over the total energy range; (b) for high- and low-energy ranges.

detected in the radio, optical and gamma-ray domain. Another difference between the two pulsars is, that the Crab pulsar reaches its maximum luminosity in the hard X-ray to soft gamma-ray range, while the Vela pulsar reaches its maximum luminosity in the few-hundred-MeV range, with only an upper limit at hard X-rays.

In the COS-B gamma-ray domain the spectrum of the Crab pulsar emission can be represented by a single power law of index 2.00±0.10 and no systematic variations of spectral index with pulsar phase have been noted, comparing three components in the Crab phase histogram: first peak, interregion, and second peak /46/. In the case of Vela the situation is markedly different: The time-averaged spectrum of the whole pulsed (no steady emission from the pulsar/nebula direction has been detected /47/) emission cannot be described by a single power law and the data show strong evidence for a spectral break at approximately 300 MeV. A two-power-law fit gives a good representation of the data with an index 1.72±0.07 (50-300 MeV) and 2.12±0.07 (300-5000 MeV). The situation becomes more complicated when the different phase intervals indicated for Vela in Figure 5b are selected: The spectra are significantly different /47/, as is shown in Figure 6. There is a clear indication that different components contribute to the total pulsed flux. This conclusion is reinforced when the evidence for long-term time variability is considered.

The search in the COS-B data for long-term variability in the emission from the Crab, showed evidence for variability at a 3 standard deviation level. Namely, the ratio of the two peaks in the pulsar's lightcurve showed variability over a time scale of years (see Figure 7), and the flux from the second pulse varies over a similar scale. For Vela, the long-term fluctuations are much more dramatic: Figure 8 shows the strong variations in gamma-ray flux in comparison with similar long-term variability at 408 MHz. These secular changes in the Vela radio flux /48/ are peculiar for radio pulsars, but a correlation with the gamma-ray variations is not evident, nor with the events of large glitches (indicated in the figure) in the pulsar's rotational parameters. Figure 9 indicates that the amount of variability is different for the selected components in the phase histogram. Clearly, the variability is largest for the components between the main peaks. Particularly remarkable are the large variatons at lower energies of the

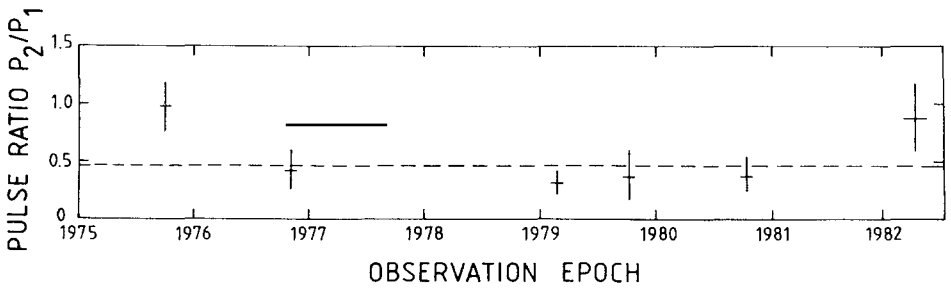

Fig.7. Temporal variation of the counts ratio of the second pulse to the first pulse of the Crab pulsar over an interval from 1975 to 1982 in the energy range 50-3000 MeV.

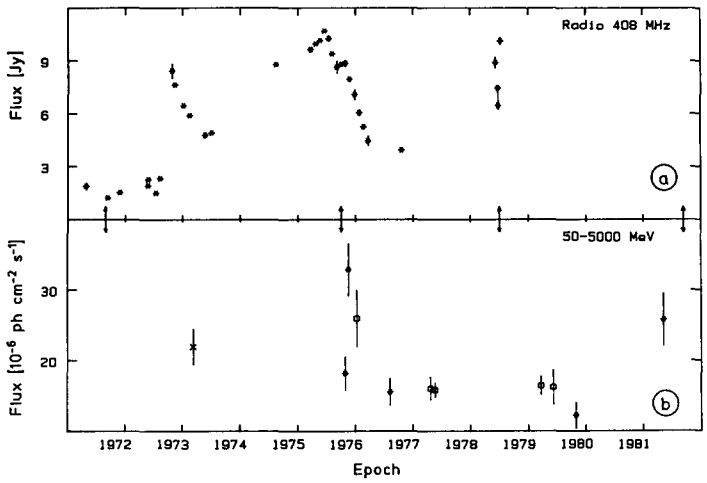

Fig.8. Comparison between the evolution of (a) the radio flux at 408 MHz /48/ and (b) the high-energy gamma-ray flux for the Vela pulsar. Gamma-ray data points from /3/ and /47/. The epochs of the pulsar glitches are indicated.

spectral shape and flux of the gamma-ray structure coinciding in phase with the first optical pulse. In conclusion: The COS-B data show that five discrete emission regions within the Vela lightcurve have been identified, with the spectral characteristics and long-term behaviour being different.

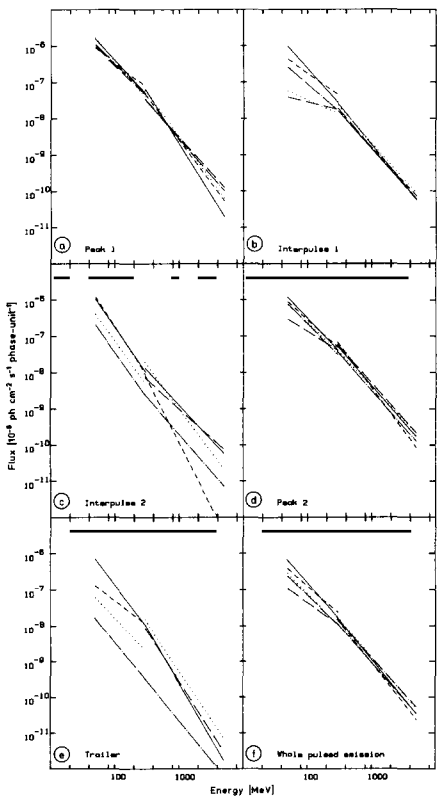

Fig.9. Differential pulsed gamma-ray spectra (50-5000 MeV) from Vela for 5 phase intervals (indicated in Figure 5) and the total phase-averaged emission. The power-law spectra giving the maximum likelihood fits /47/ are shown for the 50-300 MeV and 300-5000 MeV energy ranges, respectively, for 5 observation periods between 1975 and 1982.

These results on the Crab and Vela pulsar in gamma rays, as well as the indication for polarized gamma-ray emission from the Vela pulsar /49/ and the variation of the hard X-ray spectra with phase for the Crab (e.g. Hasinger /50/) support the idea that various source regions simultaneously exist in the pulsars magnetospheres and that the physical processes generating the gamma rays in these sites differ with the location (in altitude and latitude). It is beyond the scope of this review to discuss the different pulsar scenarios, however, it can be noticed that these detailed results from COS-B on the Crab and Vela pulsars have not yet been fully accounted for in the existing elaborative models.

REFERENCES

1. H.A. Mayer-Hasselwander et al.: 1985, Proc. 19th. Int. Cosmic Ray Conf., La Jolla, U.S.A. **3**, 383.
2. D.A. Kniffen et al.: 1974, *Nature*, **251**, 397.
3. D.J. Thompson et al.: 1977, *Ap. J. Letters*, **214**, L17.
4. D.A. Kniffen et al.: 1975, Proc. 14th Int. Cosmic Ray Conf., München, **1**, 100.
5. G.F. Bignami et al.: 1975, *Space Sci. Instr.* **1**, 245.
6. L. Scarsi et al.: 1977, Proc. 12th. ESLAB Symp. Recent Advances in Gamma-Ray Astronomy, ESA SP-124, 3.
7. W. Hermsen: 1980, Ph.D. Thesis, Leiden University.
8. J.B.G.M. Bloemen: 1985, Ph.D Thesis, Leiden University.
9. A.W. Strong et al.: 1987, *Astron. Astrophys. Suppl.*, **67**, 283.
10. J.B.G.M. Bloemen: 1989, *Ann. Rev. Astron. Astrophys.* **28**.
11. F.M. Stecker: 1971, *Cosmic Gamma Rays*, Mono Book Co., Baltimore.
12. W. Hermsen et al.: 1977, *Nature*, **269**, 494.
13. B.N. Swanenburg et al.: 1981, *Ap. J. Letters*, **242**, L69.
14. A.W. Strong et al.: 1988, *Astron. Astrophys*, **207**, 1.
15. F. Lebrun et al.: 1982, *Astron. Astrophys.*, **107**, 390.
16. A.W. Strong et al.: 1982, *Astron. Astrophys.*, **115**, 404.
17. F. Lebrun, J.A. Paul: 1985, Proc. 19th Int. Cosmic Ray Conf., La Jolla, **1**, 309.
18. J.B.G.M. Bloemen et al.: 1984, *Astron. Astrophys.*, **139**, 37.
19. W. Hermsen and J.B.G.M. Bloemen: 1983, in "Surveys of the Southern Galaxy", eds. W.B. Burton, F.P. Israel, p. 65, Reidel Publ. Comp.
20. J.B.G.M. Bloemen: 1985, *Astron. Astrophys.*, **145**, 391.
21. D.J. van der Walt, A.W. Wolfendale: 1988, *Space Science Reviews*, **47**, 1.
22. A.W. Strong: 1989, *Space Science Reviews*, in press.
23. J.B.G.M. Bloemen, L. Blitz, W. Hermsen: 1984, *Ap. J.*, **279**, 136.
24. J.B.G.M. Bloemen et al.: 1984, *Astron. Astrophys.*, **135**, 12.
25. J.B.G.M. Bloemen et al.: 1986, *Astron. Astrophys.*, **154**, 25.
26. M.R. Issa et al.: 1981, *J.Phys. G.: Nucl. Phys.*, **7**, 973.
27. C.L. Bhat, C.J. Mayer, A.W. Wolfendale: 1984, *Astron. Astrophys.*, **140**, 284.
28. C.L. Bhat et. al.: 1986, *Phil. Trans. R. Soc. London*, A **319**, 249.
29. C.L. Bhat et al.: 1985, *Nature*, **314**, 515.
30. M.J. Rogers et al: 1989, submitted; see also /21/.
31. C.E. Fichtel et al.: 1975, *Ap.J.*, **198**, 163.
32. H.A. Mayer-Hasselwander et al.: 1980, *Ann. New York Ac. of Sc.*, **336**, 211.
33. G.E. Morfill et al.: 1981, *Ap. J.*, **246**, 810.
34. J.G.A. Wouterloot: 1981, Ph. D. Thesis, Leiden University.
35. P.A. Caraveo et. al.: 1980, *Astron. Astrophys.*, **91**, L3.
36. R.J. Maddalena et al.: 1986, *AP.J.* **303**, 375.
37. E.J. de Geus: 1988, Ph. D. Thesis, Leiden University.
38. R.D. Blandford, L.L. Cowie: 1982, *Ap. J.*, **260**, 625.
39. A.M.T. Pollock: 1985, *Astron. Astrophys.*, **150**, 339.
40. B.N. Swanenburg et al.: 1978, *Nature*, **275**, 2981.
41. G.F.Bignami et al.: 1981, *Astron. Astrophys.*, **93**, 71.
42. W. Hermsen et al.: 1981, Proc. 17th Int. Cosmic. Ray Conf., Paris, **1**, 230.
43. G.F. Bignami, W. Hermsen: 1983, *Ann. Rev. Astron. Astrophys.* **21**,67.
44. A.M.T. Pollock et al.: 1985, *Astron. Astrophys.* **146**, 352.
45. A.M.T. Pollock et al.: 1985, Proc. 19th Int. Cosmic Ray Conf., La Jolla, **1**, 338.
46. J. Clear et al.: 1987, *Astron. Astrophys.* **174**, 85.
47. I.A. Grenier et al.: 1988, *Astron. Astrophys.* **204**, 117.
48. W.B. McAdam: 1981, Proc. Astron. Soc. Australia **4**, 219.